WPBB-PR(18) 21388

R Antunes et al.

Dimensioning of ideal membrane cascade systems for the separation of binary gas mixtures for nuclear fusion applications

Preprint of Paper to be submitted for publication in
Fusion Engineering and Design

This work has been carried out within the framework of the EUROfusion Consortium and has received funding from the Euratom research and training programme 2014-2018 under grant agreement No 633053. The views and opinions expressed herein do not necessarily reflect those of the European Commission.

Dimensioning of ideal membrane cascade systems for the separation of binary gas mixtures for nuclear fusion applications

R. Antunes[a,b*], L. Frances[a]

[a] *Karlsruhe Institute of Technology, Institute for Technical Physics, Tritium Laboratory Karlsruhe, Hermann-von-Helmholtz-Platz 1, D-76344 Eggenstein-Leopoldshafen, Germany*

[b] *BioIS, Biosystems & Integrative Sciences Institute, Faculdade de Ciências, Universidade de Lisboa, Campo Grande, 1749-016 Lisboa, Portugal*

Abstract

In the DEMO reactor highly efficient separation systems (> 80%) are required for the recovery of tritiated species and therefore ensure a continuous re-fuelling of the plasma. Examples of such systems are the tritium extraction system for the separation of Q_2 from He (as in the case of the European Helium Cooled Pebble Bed blanket) and the separation of DT molecules from plasma enhancement gases (e.g., Ar, Xe, ...) at the exhaust of the vacuum vessel (Q = H, D, T). For these systems, porous inorganic membranes have been proposed. However, due to the similar sizes and/or masses between the molecules, the separation of the porous membranes can be rather limited. Therefore, to comply with the performance requirements desired in a fusion reactor, multi-stage membrane systems are required. In this paper, a numerical algorithm is presented to estimate the minimum number of stages required for a relevant range of selectivities and performance requirements (i.e., enrichment factor EF and recovery fraction RF). The results show that the number of stages greatly depends on the membrane's selectivity α, EF and RF. For instance for $\alpha = 2 \rightarrow 10$ the number of stages decreases from 16 to 6 for $EF = 20$ and $RF = 90\%$. In addition, the injection flow was found to have a significant impact in the overall membrane's surface area and power consumption. At the last part of this paper the feasibility and viability of a membrane cascade system are discussed regarding to its size, power consuption and impact on the tritium inventory.

Keywords: gas separation, inorganic membranes, membrane cascade, fuel processing, nuclear fusion

1. Introduction

Mature separation technologies relying on cryogenic distillation or adsorption columns are planned to be used at ITER. For instance, cryogenic columns operated below 30 K for the separation of hydrogen isotopologues (i.e., H_2, HD, D_2, HT, DT, T_2) are foreseen to be used in the isotope separation system of the ITER fuel cycle [1, 2]. Moreover, adsorption columns relying on ZrCo getters to trap the hydrogen isotopologues and zeolite beds to remove water at 298 K are proposed to be used in the tritium extraction system of the HCPB test blanket module [3]. Although these technologies have a high readiness level, they also present some drawbacks. On the one side, the use of cryogenic temperatures lead to high operation costs, especially because large flows (i.e., purge gas) will be required for fusion reactors. On the other side, adsorption columns need to be regenerated and redundant systems are required to be operated alternatively which raises safety concerns due to the high-inventory of tritium [4]. As a matter of fact, trapping technologies are inherently non-continuous separation systems. Beyond the concerns regarding to tritium inventory, it is also an important drawback for the DEMO machine which has to demon-

*Corresponding author.

Email address: rodrigo.antunes@kit.edu (R. Antunes[a,b])

strate the tritium self-sufficiency (e.g., reactor-relevant operation times) [5]. Tritiated species that remain trapped are not available to fuel the plasma before the regeneration of the traps. Therefore, membrane technologies have been considered for the past decade as a viable and cost-effective alternative for the separation of gases in different applications [6]. Pd/Ag membranes (and membrane reactors) were also successfully developed for fusion applications since more than 20 years to continuously separate gas species in the fuel cycle of the fusion reactors [7–9]. More recently, inorganic porous membranes were also proposed for two additional applications in the European DEMO fuel cycle. First, a combination of porous inorganic membranes (e.g., zeolite-ceramic) and palladium-based membrane reactors have been considered for the tritium extraction system of the solid HCPB blanket [4]. Furthermore, porous ceramic membranes (e.g., α-Al_2O_3) have been recently proposed for the recovery of unburnt DT molecules mixed with plasma enhancement gases (e.g., Ar) coming from the torus exhaust [10]. The use of membranes technologies may ensure lower tritium inventories, improve the management of tritiated species in the fuel cycle, and guarantee continuous process operation [11]. In addition, its modularity and potential lower costs for operation are also a great benefit [12]. However, in these applications the separation efficiencies which can be achieved are usually limited since the molecules have similar diameters (e.g., the kinetic diameters of He and H_2 are, respectively, 0.26 nm and 0.289 nm). Therefore, a membrane cascade must be considered instead to achieve the separation performance required.

The number of stages integrating the membrane cascade is highly dependent on the so-called separation factor (of each stage). In addition, the required surface area for each stage is dependent on the permeances of the gases and on the feeding flow. Furthermore, since separation is driven by the pressure difference across the membrane, compressors are required between stages which impact the total power required to operate the cascade. Last but not least, all these quantities are also influenced by the overall separation requirements. The estimation of the number of stages, their surface area and the power required to operate them are crucial to discuss the feasibility and the interest of membrane cascades at reactor scale. At the best of our knowledge in the literature there is no study which presents a comprehensive analysis of the impact of these parameters (e.g., selectivity) on the cascade dimensioning for fusion applications. Thus, a model and a sensitivity analysis to support the dimensioning of membrane cascades was developed in the perspective of gas separation for fusion application, and the results are discussed with regards to feasibility and cost-effectiveness.

2. Mathematical description of an ideal membrane cascade

2.1. Definition of an ideal cascade

The classical membrane cascade arrangement consists of several separation stages placed in series, as depicted in figure 1. In this configuration, a feeding flow $F_{\mathrm{f,inj}}$ is routed to the so-called injection stage. Due to the pressure difference across the membrane, the feed flow of each stage is divided into permeate and retente flows, that are used to feed the next and previous stages, respectively. Overall, the flow $F_{\mathrm{f},i}$ feeding stage i is the sum of the retentate flow $F_{\mathrm{r},i+1}$ from stage $i+1$ and the permeate flow $F_{\mathrm{p},i-1}$ from stage $i-1$, as presented in equation (1).

$$F_{\mathrm{f},i} = F_{\mathrm{f,inj}}\delta_{\mathrm{i},inj} + F_{\mathrm{r},i+1} + F_{\mathrm{p},i-1}, \tag{1}$$

where $\delta_{i,inj} = 1$ for $i = inj$ and $\delta_{i,inj} = 0$ otherwise. f, p and r stand for feed, permeate and retentate, respectively.

The stages placed after the injection stage belong to the enriching section (N stages), whereas the stages placed before form the stripping section (M stages). The enriching section is where the enrichment of the species exhibiting the highest permeance takes place, and the stripping section is where it is depleted. Thus, the concentrations of the gas species in the flows $F_{\mathrm{r},i+1}$ and $F_{\mathrm{p},i-1}$ (which both feed stage i) will be necessarily different, and thus dilution of previously concentrated streams will occur. As a consequence, energy spent in separating the

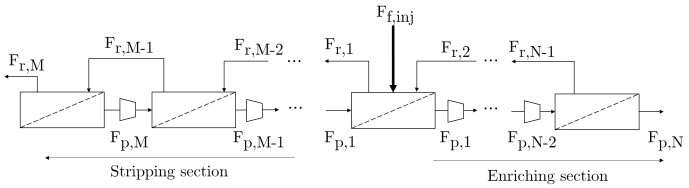

Figure 1: Schematic diagram of a membrane cascade in series arrangement. The enriching section is where the species with the highest permeance is enriched, and the stripping section is where this species is depleted.

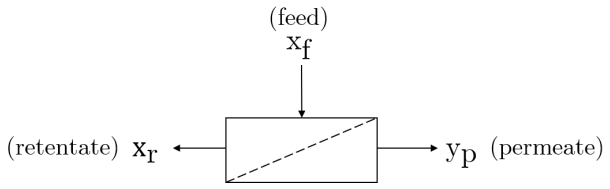

Figure 2: Single stage diagram, specifying the feed, permeate and retentate sides of the membrane with the corresponding concentrations: x_f, y_p, x_r.

gaseous species is wasted due to this dilution. Therefore, to ensure the minimum separation energy, the concentrations in the streams coming from $i + 1$ (i.e., $x_{\mathrm{r},i+1}$) and $i - 1$ (i.e., $y_{\mathrm{p},i-1}$) must be equal to the feed concentration $x_{\mathrm{f},i}$, as expressed by equation (2). This equation expresses the condition for an ideal cascade [13].

$$x_{\mathrm{f},i} = x_{\mathrm{r},i+1} = y_{\mathrm{p},i-1}, \tag{2}$$

2.2. Stage separation factor

The separation factor is a dimensionless parameter which quantifies the separation efficiency of a membrane for two different gas species. Three different separation factors, presented in equations (3) – (5), are commonly used in the literature. S_stg, which relates the permeate (y_p) and retentate (x_r) concentrations, is the stage separation factor; h, relating the permeate and feed (x_f) concentrations, is the head separation factor; t, defined by the feed and retentate concentrations, is the tail separation factor (refer to figure 2). For a separator with one inlet, it can be shown that $h = t$ leading to the relation presented in equation (6) holds [13].

$$S_\mathrm{stg} = \frac{\frac{y_\mathrm{p}}{1-y_\mathrm{p}}}{\frac{x_\mathrm{r}}{1-x_\mathrm{r}}} \equiv \frac{Y_\mathrm{p}}{X_\mathrm{r}} \tag{3}$$

$$h = \frac{\frac{y_\mathrm{p}}{1-y_\mathrm{p}}}{\frac{x_\mathrm{f}}{1-x_\mathrm{f}}} \equiv \frac{Y_\mathrm{p}}{X_\mathrm{f}} \tag{4}$$

$$t = \frac{\frac{x_\mathrm{f}}{1-x_\mathrm{f}}}{\frac{x_\mathrm{r}}{1-x_\mathrm{r}}} \equiv \frac{X_\mathrm{f}}{X_\mathrm{r}} \tag{5}$$

$$S_\mathrm{stg} = h \times t = h^2 = t^2 \tag{6}$$

Using (6) and the defintions of h and t, two relations, given by equations (7) and (8), can be derived for y_p and x_r depending solely on x_f and S_stg.

$$y_\mathrm{p} = \frac{\sqrt{S_\mathrm{stg}} X_\mathrm{f}}{1 + \sqrt{S_\mathrm{stg}} X_\mathrm{f}} \tag{7}$$

$$x_\mathrm{r} = \frac{\frac{X_\mathrm{f}}{\sqrt{S_\mathrm{stg}}}}{1 + \frac{X_\mathrm{f}}{\sqrt{S_\mathrm{stg}}}} \tag{8}$$

2.3. Ideal selectivity and pressure ratio

The separation factor, introduced in the previous section, quantifies the separation efficiency of one gas with respect to the other. Furthermore, there is another quantity which gives a first estimation for the separation performance of a permeable membrane, and it is defined by the ratio of the permeances Π_i of two gaseous species a and b (equation (9)). This quantity is defined such that it is larger than 1. Thus, according to (9), species a is enriched in the enriching section of the cascade, and depleted in the stripping section.

$$\alpha \equiv \frac{\Pi_\mathrm{a}}{\Pi_\mathrm{b}} \tag{9}$$

The permeation of gas species across a membrane is driven by the partial pressure difference between the feed and permeate sides of the membrane. Therefore, the enrichment attainable in a single separation unit is not only limited by the permselectivty α but also limited by the feed-to-permeate pressure-ratio γ defined in equation (10). It can be shown that the permeate concentration y_p obtained by feeding a membrane with a feed

concentration x_f depends on both α and γ according to equation (11) [14]. This relation is actually obtained for an idealized case of well-mixed mixtures, where the concentrations of the species are constant along the membrane module. In other words, the mixing rate of the species is considered to be much higher than their diffusion rates [15].

$$\gamma \equiv \frac{P_f}{P_p} \tag{10}$$

$$y_p = \frac{\gamma}{2}\Bigg[x_f + \frac{1}{\gamma} + \frac{1}{\alpha - 1} - \sqrt{\left(x_f + \frac{1}{\gamma} + \frac{1}{\alpha - 1}\right)^2 - 4\frac{\alpha x_f}{(\alpha - 1)\gamma}}\Bigg], \tag{11}$$

In figure 3 the permeate concentration, given by equation (11), is plotted against the pressure-ratio γ for different selectivities α. Two regimes can be identified: (i) selectivity-limited when $\alpha << \gamma$ and (ii) pressure-limited when $\gamma << \alpha$. For low selectivities (e.g., $\alpha \leq 3$), the permeate concentration increases for rather small values of γ and eventually reaches a plateau where a further increase of γ (i.e., increase of the driving force) does not lead to an increase of the enrichment. At these conditions, the increase in the permeate concentration is selectivity-limited. When the selectivity α is increased, the range where y_p is dependent on γ is wider. At these conditions, the concentration in the permeate side is limited by the pressures across the stage. A yellow region is displayed between $\gamma = 2$ and $\gamma = 20$ in the same figure to indicate the practical range of values which can be applied, considering the pumping systems availability and economical viability [14, 16]. In this region, both situations (i.e., pressure limited and selectivity limited) occur, showing that both the impact of γ and α on the membrane performances have to be considered.

Figure 4 depicts the plot of y_p as a function of α for $\gamma = 20$, considered as the maximum available of pressure-ratio currently achievable. Despite the high selectivities (i.e., $\alpha > 100$), the maximum achievable permeate concentration, for an initial concentration of 2 mol%, is limited to 4 mol%. In this case, the use of membranes with selectivities above 100 would be of marginal advantage, since its performance would be significantly limited by γ.

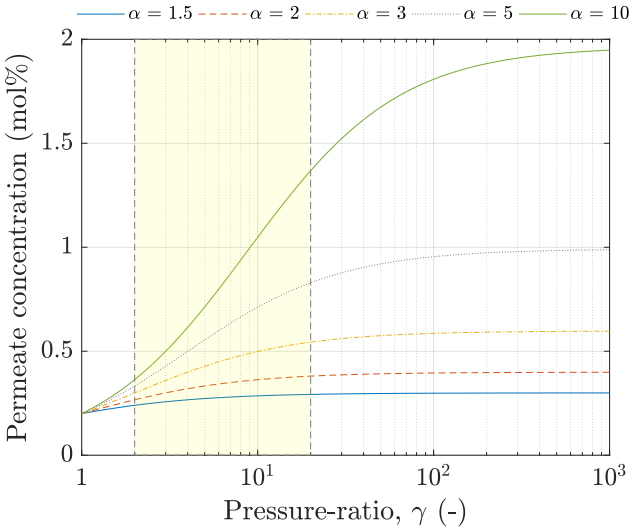

Figure 3: Permeate concentration as a function of the pressure-ratio for different selectivity values, obtained for $x_f = 0.2$ mol%. In yellow, the region for the practical pressure-ratio values is presented. $\alpha = 1.5$: solid blue line; $\alpha = 2$: dashed orange line; $\alpha = 3$: dot-dashed dark yellow line; $\alpha = 5$: dotted purple line; $\alpha = 10$: solid green line.

In addition, it can be shown (refer to Appendix A for derivation) that the separation factor S_{stg} (equation 6) depends on both α and γ via equation (12) [17]. From this equation it can be easily seen that when $\gamma \to \infty$, then $S_{stg} \to \alpha$, and the highest performance is attained. On the contrary, when $\gamma \to 1$, $S_{stg} \to 1$, and thus no separation takes place. Therefore, in practice, the range of the stage separation factor is between 1 and α.

$$S_{stg} = \frac{\alpha - y_p(\alpha - 1)\gamma^{-1}}{1 + (1 - y_p)(\alpha - 1)\gamma^{-1}} \tag{12}$$

2.4. Enrichment factor and recovery fraction

The selectivity is a well-established parameter which is used to compare and discuss separation performance of membranes. Nevertheless, for industrial applications, especially those relying on membrane cascades, two additional parameters are used to express their performance: the enrichment factor (EF) and the recovery fraction (RF). The enrichment factor, given by equation (13), quantifies the increase in concentration of the desired product at the last stage of the cascade (N in figure 1) in

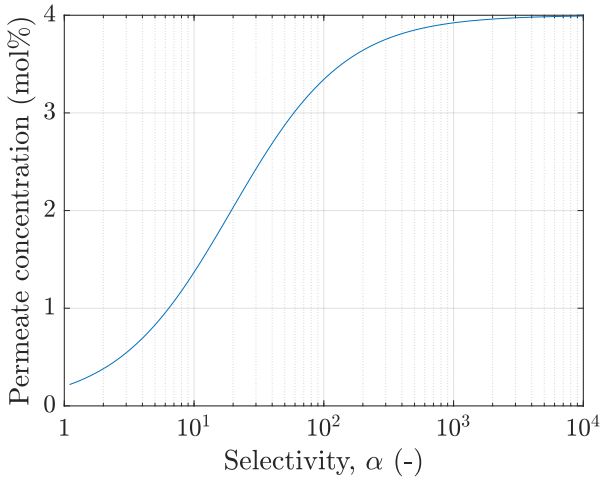

Figure 4: Permeate concentration as a function of the selectivity for $\gamma = 20$ and $x_f = 0.2$ mol%.

respect to the concentration of the initial feeding flow at the injection stage. The recovery fraction RF, given by equation (14), is the relative amount of product extracted at the last stage N in respect to the injection stage. These two quantities are used as requirements for the design and dimensioning of a membrane cascasde (e.g., to determine the required number of stages), as discussed below.

$$EF = \frac{y_{p,N}}{x_{f,inj}} \tag{13}$$

$$RF(\%) = 100 \times \frac{y_{p,N}}{x_{f,inj}} \frac{F_{p,N}}{F_{f,inj}} \tag{14}$$

2.5. Determination of the number of stages, concentrations and flows

The number of stages of a membrane cascade can be determined from the performance requirements EF and RF, the initial feed concentrations $x_{f,inj}$ and feed flow $F_{f,inj}$. The required flows and concentrations at the permeate side of stage N (i.e., the last of the enriching section), $F_{p,N}$ and $y_{p,N}$, and at the retentate side of M (i.e., the last stage of stripping section), $F_{r,M}$ and $x_{r,M}$, are determined by equations (15)-(18). Then, the number of stages is found by iterating y_p and x_r concentrations along the cascade using equations (7) and (8) until $y_p \geq y_{p,N}$ and $x_r \leq x_{r,M}$. In these equations, the X_f term is determined by the feeding concentration (equation (2)). The numerical implementation of these equations is presented and discussed in section 3.

$$F_{p,N} = \frac{1}{EF} \frac{RF}{100} F_{f,inj} \tag{15}$$

$$F_{r,M} = F_{f,inj} - F_{p,N} \tag{16}$$

$$y_{p,N} = x_{f,inj} EF \tag{17}$$

$$x_{r,M} = \frac{F_{f,inj} x_{f,inj} - F_{p,N} y_{p,N}}{F_{r,M}} \tag{18}$$

The feed flows at the inlet of each stage along the cascade are determined from the stage-cut values ν_i. The stage-cut value is defined by the permeate-to-feed flows ratio, and it can be calculated using the feed, permeate and retentate concentrations at stage i according to equation (19) (refer to Appendix B for derivation) [17]. Since $F_{p,i-1} = \nu_{i-1} F_{f,i-1}$ and $F_{r,i+1} = (1 - \nu_{i+1}) F_{f,i+1}$, equation (1) can be re-written as equation (20). The application of equation (20) to each stage results in a matrix, given by equation (21), that enables the calculation of the feed flows at the inlet of each cascade stage. The corresponding permeate and retentate flows can be calculated using, respectively, equations (22) and (23).

$$\nu_i = \frac{F_{p,i}}{F_{f,i}} = \frac{x_{f,i} - x_{r,i}}{y_{p,i} - x_{r,i}} \tag{19}$$

$$F_{f,i} = F_{f,inj} \delta_{i,inj} + (1 - \nu_{i+1}) F_{f,i+1} + \nu_{i-1} F_{f,i-1} \tag{20}$$

$$\begin{bmatrix} \vdots \\ F_{f,i-1} \\ F_{f,i} \\ F_{f,i+1} \\ \vdots \end{bmatrix} = \begin{bmatrix} \vdots & \vdots & 0 & 0 & 0 \\ -\nu_{i-2} & 1 & -(1-\nu_i) & 0 & 0 \\ 0 & -\nu_{i-1} & 1 & -(1-\nu_{i+1}) & 0 \\ 0 & 0 & -\nu_i & 1 & -(1-\nu_{i+2}) \\ 0 & 0 & 0 & \vdots & \vdots \end{bmatrix}^{-1} \begin{bmatrix} \vdots \\ \vdots \\ F_{f,inj} \\ \vdots \\ \vdots \end{bmatrix} \tag{21}$$

$$\mathbf{F}_p = \nu \mathbf{F}_f \tag{22}$$

$$\mathbf{F}_\mathrm{r} = \mathbf{F}_\mathrm{f} - \mathbf{F}_\mathrm{p} \tag{23}$$

2.6. Stages surface area

The required surface area A_i (m^2) for each stage is determined according to equation (24). This quantity depends on the total permeating flow $F_{\mathrm{p},i}$, feed and permeate pressures (i.e., γ and p_p), and gas permeance Π ($\mathrm{mol\,m^{-2}\,s^{-1}\,Pa^{-1}}$) through the membrane. The permeance is dependent on the gas type, membrane's material and temperature. The value of the permeance used to calculate the surface area is determined using the linear combination of the permeances for the two species a and b present in the stream, according to equation (25) [18].

$$A_i = \frac{F_{\mathrm{p,i}}}{\Pi p_\mathrm{p}(\gamma - 1)} \tag{24}$$

$$\Pi = \Pi_\mathrm{a} x_{\mathrm{f,a}} + \Pi_\mathrm{b} x_{\mathrm{f,b}} \tag{25}$$

2.7. Evaluation of the compression power

As presented in figure 1, compressors are employed between stages to increase the pressure of the flow routed from the permeate side of stage i to the feed side of stage $i+1$, and maintain a sufficient pressure difference across the membranes of the different stages. The compression power required is dependent on the minimum molar energy W_min ($\mathrm{J\,mol^{-1}}$) required to isentropically compress a gas from p_p to p_f [19]. W_min is determined by equation (26), where c_p and c_v are the gas specific-heat constants ($\mathrm{J\,K^{-1}\,kg^{-1}}$), T is its temperature (K) and R is the constant for ideal gases ($\mathrm{J\,K^{-1}\,mol^{-1}}$).

$$W_\mathrm{min} = RT\frac{c_\mathrm{p}}{c_\mathrm{p} - c_\mathrm{v}}\left[\left(\frac{p_\mathrm{f}}{p_\mathrm{p}}\right)^{\frac{c_\mathrm{p}}{c_\mathrm{p}-c_\mathrm{v}}}\right] \tag{26}$$

The total compressing power P_tot (W) required to run the membrane cascade can be calculated by summing all the contributions for the $N+M-1$ stages (the permeate flow of the N-th stage is not compressed), as expressed by equation (27). The electrical-to-mechanical conversion efficiency η is also considered, which is typically around 70% [20].

$$P_\mathrm{tot} = \frac{W_\mathrm{min}}{RT\eta}\left(\sum_{i=1}^{M} F_{\mathrm{p,i}} + \sum_{j=1}^{N-1} F_{\mathrm{p,j}}\right) \tag{27}$$

3. Numerical implementation

The objective of this work is to determine numerically the number of stages required to achieve a defined set of separation performance, given by the enrichment factor and recovery fraction defined in equations (13) and (14). In addition, the gas concentrations and flows along the cascade, the stages' surface area and power consumption are also desired outputs of the numerical calculations (since they have a direct impact on the physical dimensioning and operating costs). These parameters are calculated relying on a simple algorithm. The required input parameters for these calculations are: enrichment factor (EF) and recovery fraction (RF), feed flow at the injection stage ($F_\mathrm{f,inj}$) and concentrations ($x_\mathrm{f,inj}$) of the binary mixture feeding flow, feed-to-permeate pressures (γ) and permeances ratio given by the selectivity α. The numerical implementation follows the steps below:

a) with EF, RF, $F_\mathrm{f,inj}$ and $x_\mathrm{f,inj}$, determine the permeate and retentate concentrations of the most permeating species: $y_\mathrm{p,N}$ (equation (17)) and $x_\mathrm{r,M}$ (equation (18));

b) using α, γ and $y_\mathrm{p,N}$, estimate the stage separation factor S_stg, given by equation (12);

c) with S_stg and $x_\mathrm{f,inj}$, determine the permeate ($y_\mathrm{p,stg}$) and retentate ($x_\mathrm{r,stg}$) concentrations of the injection stage, with equations (7) and (8);

d) using the feed, permeate and retentate concentrations for the injection stage, calculate its cut-value ν_stg, using equation (19);

e) using $y_\mathrm{p,stg}$ as feed concentration for stage 1 of the enriching section, use $X_\mathrm{f} = \frac{y_\mathrm{p,stg}}{1-y_\mathrm{p,stg}}$ to determine $y_\mathrm{p,1}$ and $x_\mathrm{r,1}$ (as in step c)). Repeat these calculations until the permeate concentration has an equal or larger value than $y_\mathrm{p,N}$. The number of iterations required is equal to the number of stages N in the enriching section. For each stage determine the cut-values as described step d);

f) using $x_{r,1}$ as feed concentration for stage 1 of the stripping section, use $X_f = \frac{x_{r,1}}{1-x_{r,1}}$ to determine $y_{p,1}$ and $x_{r,1}$ (as in step c)). Repeat these calculations until the retentate concentration has an equal or lower value than $x_{r,M}$. The number of iterations required is equal to the number of stages M in the stripping section. For each stage determine the cut-values as described in step d);

g) the feed flows along the cascade are determined using the cut-values ν_i in the matrix equation (21). The permeate and retentate flows are then calculated using, respectively, (22) and (23);

h) using the permeate flows determined in g), the gamma-value, the permeate pressure, and the permeances of the permeating gases, the surface area of each stage can be determined with equation (24). The total compressing power is also calculated using the permeate flows, according to equation (27).

4. Sensitivity analysis for membrane cascade dimensioning

4.1. Input and output parameters

In the sensitivity study presented below, we are interested in determining the impact of the required performance (EF, RF), operating conditions (γ) and membrane properties (α) on the:

- number of stages N and M;
- stages flows $F_{f,i}$, $F_{p,i}$ and $F_{r,i}$;
- stages surface areas A_i;
- total power consumption P_{tot}.

These four characteristics of the membrane cascade were selected as they provide key information regarding its design, dimensions and cost-effectiveness, required to evaluate the feasibility of membrane technology for a given application.

For the sensitivity analysis a reference case is considered, whose scenario is presented in table 1. The values $EF = 20$ and $RF = 90\%$ were proposed in an earlier publication for the performance of the membrane cascade in DEMO-relevant conditions for the HCPB TER system [21]. The composition of the purge gas downstream of the breeding blanket is expected to consist mainly of H_2 and He, with 0.1 wt.% H_2/He (which translates into 0.2 mol% H_2/He) [22]. In addition, $\alpha = 2$ is representative of the selectivity value obtained by calculating the ratio of the experimental permeances of H_2 and He obtained for a MFI zeolite-type membrane, also given in table 1 [23]. From this reference case, EF, RF, α and γ are varied in ranges of interest and their impact on the dimensioning of the cascade is discussed. For the sensitivity analysis, the stages are numbered $1, 2, ..., N_{stg}$, where N_{stg} corresponds to the total number of stages (i.e., $N_{stg} = N + M + 1$).

Symbol	Value	Unit
EF / RF	20 / 90%	–
H_2 / He	0.2 / 99.8	mol%
Π_{H2}	0.72	μmol m^{-2}s^{-1}Pa^{-1}
Π_{He}	0.34	μmol m^{-2}s^{-1}Pa^{-1}
α	2	–
$F_{f,inj}$	10^4	m^3 h^{-1} at STP

Table 1: Reference case parameters used for the sensitivity analysis based on the requirements for the TER system of the EU-DEMO [21, 22]. The permeances for H_2 and He were obtained experimentally with zeolite membranes [23]. STP: standard conditions for temperature and pressure.

4.2. Influence of selectivity and pressures-ratio

4.2.1. Number of stages

In figure 5, the number of stages as a function of α, obtained for $EF = 20$ and $RF = 90\%$ is presented. This plot was obtained for $\gamma = 20$ (i.e., upper limit of the realistic pressure-ratio values discussed in section 2.3). The total number of stages decreases from 27 for $\alpha = 1.5$ down to 6 for $\alpha = 10$. It should be noticed that the number of stages sharply decreases from 27 down to 9 when the selectivity increases from $\alpha = 1.5$ to $\alpha = 4$. When the selectivity is increased further to 10, only three stages are spared.

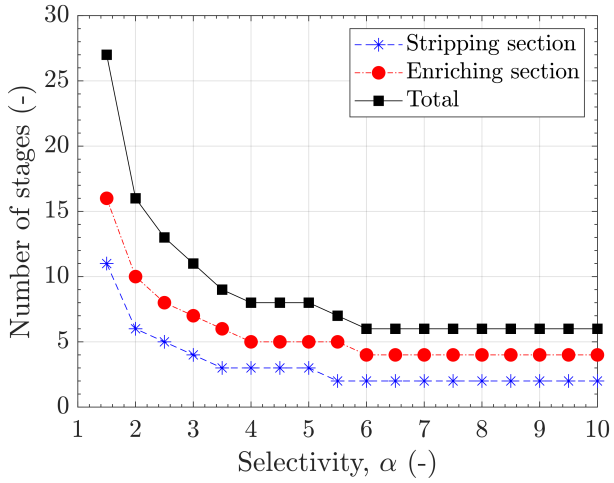

Figure 5: Number of stages as a function of the selectivity. Obtained for $\gamma = 20$, $EF = 20$, $RF = 90\%$. Stages in stripping section: dashed blue line with stars; stages for enriching section: dot-dashed red line with circles; total number of stages (i.e., enriching plus stripping): solid black line with squares.

The number of stages obtained with $\gamma = 20$ is the smallest that would be required for practical applications. However, this value corresponds to the largest power consumption required which directly impacts the feasibility of the system. Therefore, an investigation was done to determine, for each selectivity α, what is the minimum value γ_{min} which keeps the number of stages at a minimum. The results are compiled in table 2. For each selectivity, a range $[\gamma_{\text{min}}, \gamma_{\text{max}}]$ was determined, corresponding to the pressure ratios that can be applied without changing the number of stages. The resulting range for the stage separation factors $[S_{\text{stg,min}}, S_{\text{stg,max}}]$, calculated with (3), are also presented.

For selectivites between 6 and 10, the minimum number of stages required to achieve $EF = 20$ and $RF = 90\%$ is the same and equal to 6. Nevertheless, γ_{min} decreases when the selectivity increases. For instance, $\gamma_{\text{min}} = 7.5$ for $\alpha = 10$. Therefore, although there is no reduction of the total number of stages, the increasing of selectivity relaxes the required pressure-ratio. It is also interesting to appreciate that for low selectivities, S_{stg} and α are very similar, whereas, for instance, for $\alpha = 10$ S_{stg} is not larger than 6.9. This illustrates the two regimes introduced in section 2.3 (pressure and selectivity limited).

α (-)	N_{stg} (-)	γ_{min} (-)	γ_{max} (-)	$S_{\text{stg,min}}$ (-)	$S_{\text{stg,max}}$ (-)
1.5	27	19.0	20.0	1.462	1.464
2	16	11.5	20.0	1.843	1.906
3	11	9.5	20.0	2.489	2.734
4	8	16.0	20.0	3.383	3.491
5	8	8.5	20.0	3.431	4.188
6	6	16.0	20.0	4.606	4.831
7	6	11.5	20.0	4.650	5.425
8	6	9.5	20.0	4.668	5.977
9	6	8.5	20.0	4.708	6.491
10	6	7.5	20.0	4.624	6.971

Table 2: Range of γ, and corresponding range of S_{stg}, for which the lowest practical number of stages is ensured for $EF = 20$, $RF = 90\%$ and $x_{\text{f,i}} = 0.2$ mol%.

4.2.2. *Flows and concentrations*

As discussed in section 2.1, the classical membrane cascade is operated under flows circulating between stages. As a consequence, there is a build-up of flows along the cascade, whose steady-state profile can be determined from the equations presented before. The profile for the feed flows is presented in figure 6. This plot was obtained for the conditions presented in table 1, which provides a 16-stages cascade, and the feeding stage is the number 7. It should be noticed that, as a result of the build-up of flows, the flow at the injection stage is around 5.4×10^4 m^3/h, which is roughly five times higher than the initial feeding flow. However, the retentate and permeate flows $F_{\text{r,1}}$ and $F_{\text{p,16}}$ are, respectively, 9626 m^3/h and 374 m^3/h, and thus the mass-balance is respected. This asymetric profile of the feed flows is explained by the fact that a small fraction of the feeding flow permeates through the membrane stages, where a large fraction is recycled back in the retentate sides of the stages (i.e., $\nu_i < 0.5$). As a result, larger flows exist at the stripping section in comparison to the enriching section.

The plot of figure 7 shows the total feed flow at the injection stage as a result of the recycling of flows between stages,

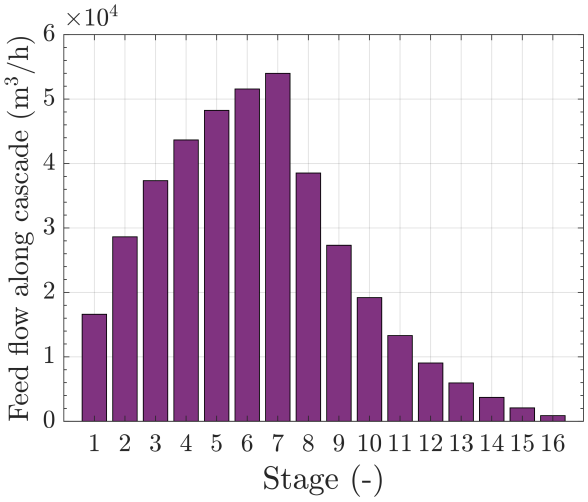

Figure 6: Feed flow along the cascade stages. Obtained for $EF = 20$, $RF = 90\%$, $F_{\mathrm{f,inj}} = 10^4\,\mathrm{m^3/h}$, $\gamma = 20$ and $\alpha = 2$. The 7-th stage is the injection stage.

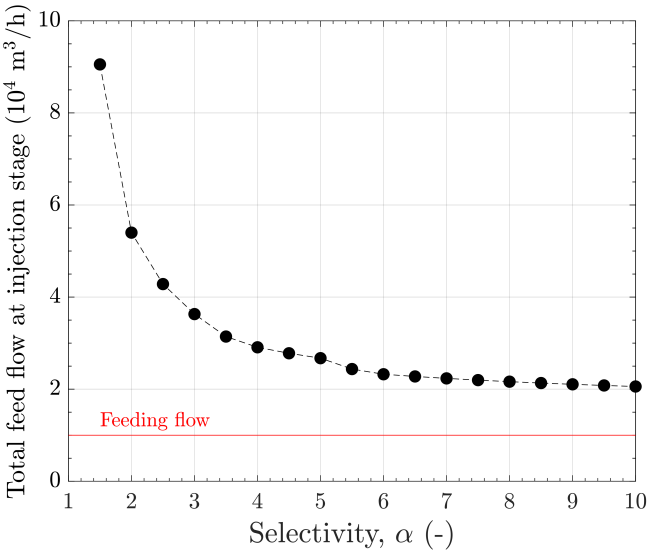

Figure 7: Feed flow at the injection stage as a function of the selectivity. The red solid line indicates the original feed flow: $F_{\mathrm{f,inj}} = 10^4\,\mathrm{m^3/h}$. Obtained for $EF = 20$, $RF = 90\%$ and $\gamma = 20$.

obtained for $F_{\mathrm{f,inj}} = 10^4\,\mathrm{m^3/h}$. Since the number of stages decreases with the selectivity (figure 6), the build-up of flows also decreases. While for $\alpha = 1.5$ the feed flow amounts to roughly 9 times the initial feeding flow, for $\alpha = 10$ the total feed flow is only 2 times higher than $F_{\mathrm{f,inj}}$. Thus, considering that the initial feeding flow foreseen to purge the breeding blanket is already large, the use of a membrane cascade would increase this flow at least two times ($2 \times 10^4\,\mathrm{m^3/h}$ in this case). This fact raises questions regarding to the dimensions and footprint of the system (i.e., components, pipework) but also to tritium inventory (even though membrane cascades can be operated continuously and do not require a redundant system). These aspects are discussed in section 5.

The plot of figure 8 shows the profiles of the feed, permeate and retentate concentrations along the cascade for the species with the highest permeance. These results were obtained for the reference case. As expected, the concentrations increase along the cascade, towards the last stage of the enriching section, where the highest concentrations are obtained. The retentate concentration at stage 1 and the permeate concentration at stage 16 meet the input requirements presented in section 2.5: the permeate concentration at stage 16 is 4.79 mol%, which is higher than $y_{\mathrm{p,N}} = 4\,\mathrm{mol\%}$ (using equation (13)); the retentate concentration at stage 1 is 0.015 mol%, which is lower than $x_{\mathrm{r,M}} = 0.021\,\mathrm{mol\%}$ (using equation (18)). Furthermore, it should be noticed that the permeate and retentate concentrations of stages $i-1$ and $i+1$, respectively, are equal to the feed concentration at stage i (as expected from the definition of ideal cascade, given by equation (2)).

4.2.3. Permeate flow at the last stage

In view of the applicability of a membrane cascade in a complex system such as the fuel cycle of a fusion reactor, with plenty of interfaces, the permeation flow $F_{\mathrm{p,N}}$ at the last stage (and/or the retentate flow $F_{\mathrm{r,M}}$ at the first stage) is a very important parameter to take into account. This flow will have a direct impact on the dimension of the next system, or, conversely, the existence of an interface may impose important constraints on the flows and concentrations which have to be reached downstream of the cascade. In the plot of figure 9, the ratio $F_{\mathrm{p,N}}/F_{\mathrm{f,inj}}$ is plotted as a function of the selectivity for $EF = 20$, $RF = 90\%$ and $\gamma = 20$. The dependency of the relative permeate flow with the selectivity is not monotonic because the number of stages required to fulfill EF and RF also changes with the selectivity (refer to section 4.2.1 and figure 5).

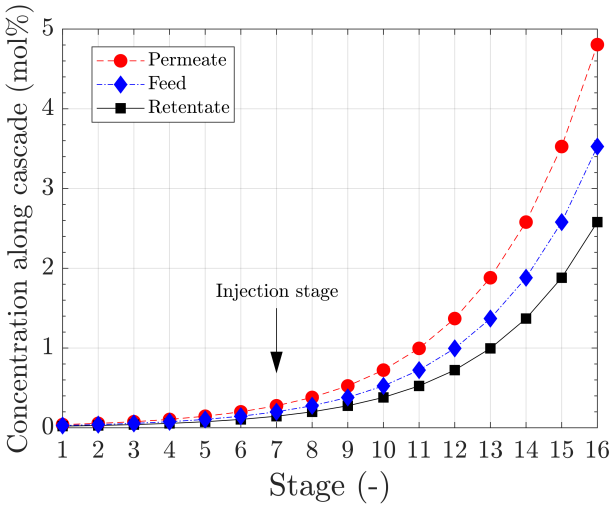

Figure 8: Absolute concentrations of the most permeating species along the cascade stages, obtained for $EF = 20$, $RF = 90\%$, $\gamma = 20$, $\alpha = 2$ and $x_{f,i} = 0.2\,\text{mol}\%$. Feed: blue dot-dashed line with diamonds; Permeate: red dashed line with circles; Retentate: black solid line with squares.

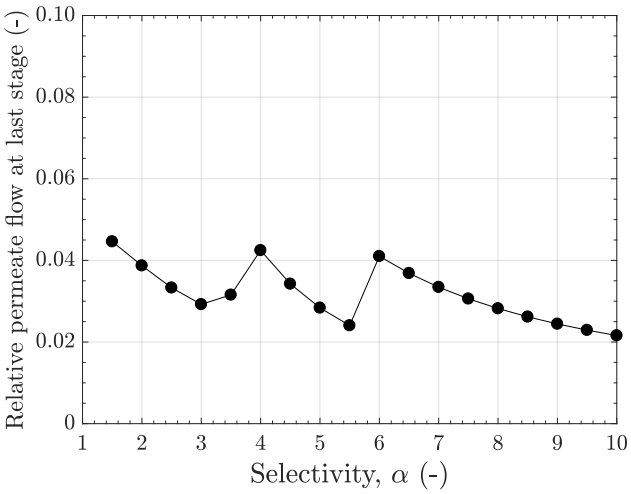

Figure 9: Relative permeate flow at last stage, in respect to the feed flow F_f, as a function of the selectivity α. Obtained for $\gamma = 20$, $EF = 20$, $RF = 90\%$, $F_{f,inj} = 10^4\,\text{m}^3/\text{h}$.

For selectivity ranges associated to a constant number of stages ($\alpha = 6 - 10$, with 6 stages), the relative permeate flow at the last stage decreases with the selectivity. As a matter of fact, a higher selectivity induces a decrease of the permeate flow (and an increase of the retentate flow).

For α values between 6 and 10 the total number of stages is constant, and equal to 6 (refer to figure 5). Therefore, when α increases, the concentration of the most permeating species in the permeate flow increases, leading to a decrease of the total permeate flow: from roughly 4% down to 2% of the injection feed flow. Likewise, for $\alpha = 4 - 5$, the number of stages is also constant (equal to 8) resulting in a decrease of $F_{p,N}$ with α. For selectivities between 1.5 and 3.5, the relative permeate flow at last stage globally decreases but is impacted by additional effects, as the number of stages is reduced from 27 to 9.

Regardless of the selectivity, the permeate flow at the last stage of the enriching section represents only a small percentage of the initial feeding flow (in the range $2\% - 5\%$), whereas the retentate flow of the first stage contribution is above 90%. Nevertheless, these values change considerably with EF, as it is shown in section 4.3.2. In view of the application of the membrane cascade to the TER system of the HCPB, the depleted, large flow at the retentate side of the stripping section is re-used for further purging of the ceramic beds. The enriched, small flow of the enriching section is used as input for the membrane reactor, which must be kept at reasonable size and costs.

4.2.4. *Surface area*

The total surface area of each membrane cascade system as a function of the selectivity is presented in the figure 10 for $\gamma = 20$. A monotonic decrease of the area exists from $\sim 1 \times 10^4\,\text{m}^2$ for $\alpha = 1.5$ down to $\sim 3 \times 10^2\,\text{m}^2$ for $\alpha = 10$, mainly due to the decreasing number of stages. If the minimized pressure-ratios (γ_{min} in table 2) would have been used instead, the surface area would be greater (up to five times). This fact demonstrates the trade-off existing between the pressure-ratio (i.e., compression power) and the surface area. Moreover, calculations with different injection flows highlight its strong impact on the surface area: a flow decrease by a factor of 10, would lead to 10 times less area.

4.2.5. *Power consumption*

The total power consumption of each membrane cascade system as a function of the selectivity was calculated using equation (27) and is presented in figure 11 for $\gamma = 20$. A

sharp decrease exists from $\sim$ 120 MW for $\alpha = 1.5$ down to $\sim$ 4 MW for $\alpha = 10$, which corresponds to a power reduction by a factor of 30. The order of magnitude for the power consumption is essentially determined by the flows. Therefore, the flow-independent power consumption reduction relative to $\alpha = 1.5$ is also presented in figure 11. From $\alpha = 1.5$ to $\alpha = 3.5$, the power consumption is reduced by one order of magnitude. Further increasing of α to 10, the power required is only reduced by a factor 3. If the γ_{min} values (table 2) would have been used as input, the power consumption could be reduce by, at best, a factor of 2. As for the surface-area, if the injection flow is decreased by a factor 10 the power also reduces by the same factor (equation 27).

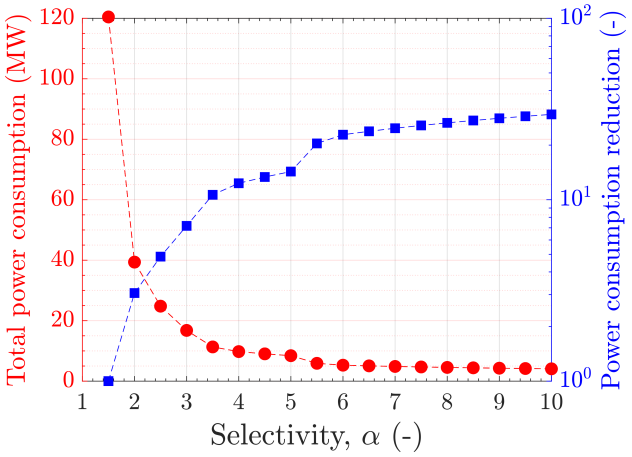

Figure 11: Total power consumption (red dashed-line with circles) and power reduction (in respect to the value for $\alpha = 1.5$, blue dashed-line with squares) as a function of the selectivity α for $\gamma = 20$. Obtained for $EF = 20$, $RF = 90\%$, $F_{\text{f,inj}} = 10^4$ m^3/h.

4.3. Influence of EF and RF

4.3.1. Number of stages

The number of stages as a function of both EF and for different values of RF, both used as performance requirements defined in equations (13) and (14), is presented in the plot of figure 12 for $\alpha = 2$ and $\gamma = 20$. The total number of stages (top plot) varies considerably with both EF and RF. On the one side, for higher values of EF a higher purification is required, and thus more stages are required in the enriching section (middle plot in the same figure). For instance, for $RF = 90\%$, the number of stages increases from 14, for $EF = 10$, to 22, for $EF = 90$. On the other side, for a constant value of EF and a given injection flow, a higher RF can only be reached by increasing the permeate flow at the output of the cascade, which is achieved by increasing the number of stages to promote an increase of the buid-up flows (equation 14). As EF is constant, the number of stages in the enriching section is kept constant, and hence the number of stages in the stripping section increases. This behavior can be appreciated in the middle and bottom plots of figure 12. The number of stages in the stripping section is mainly driven by RF, whereas the stages in the enriching section is independent of RF. Moreover, it should be noted that the impact of RF on the total number of stages is greater when $RF \rightarrow 100\%$. In fact, by increasing RF from 80% to 90%, the total number of stages for $EF = 20$ increases by 3, while from 90% to 99% the increase in number of stages is 7. Increasing further RF the number of stages required increases dramatically. At the limit of 100% an infinite number of stages would be required. This is justified by the fact that the cascade consists of membranes permeable for the feeding species, and thus a complete recovery of the desired product is not possible.

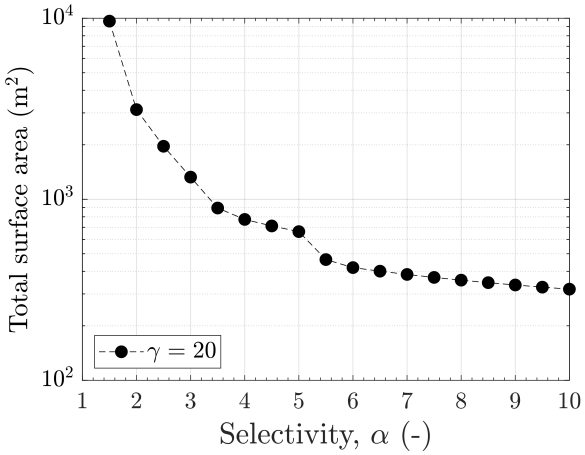

Figure 10: Total surface area as a function of the selectivity for $\gamma = 20$. Obtained for $EF = 20$, $RF = 90\%$, $\alpha = 2$ and $F_{\text{f,inj}} = 10^4$ m^3/h.

In the plot of figure 13, the total number of stages for $\alpha = 10$ as a function of both EF for different RF values is presented. It can be observed that the impact of EF and RF on the number

of stages is significantly lower than it is for $\alpha = 2$, since the stages have a high selectivity: for $RF = 90\%$, the number of stages increases from 5 to 7 when EF increases from 10 to 90, respectively.

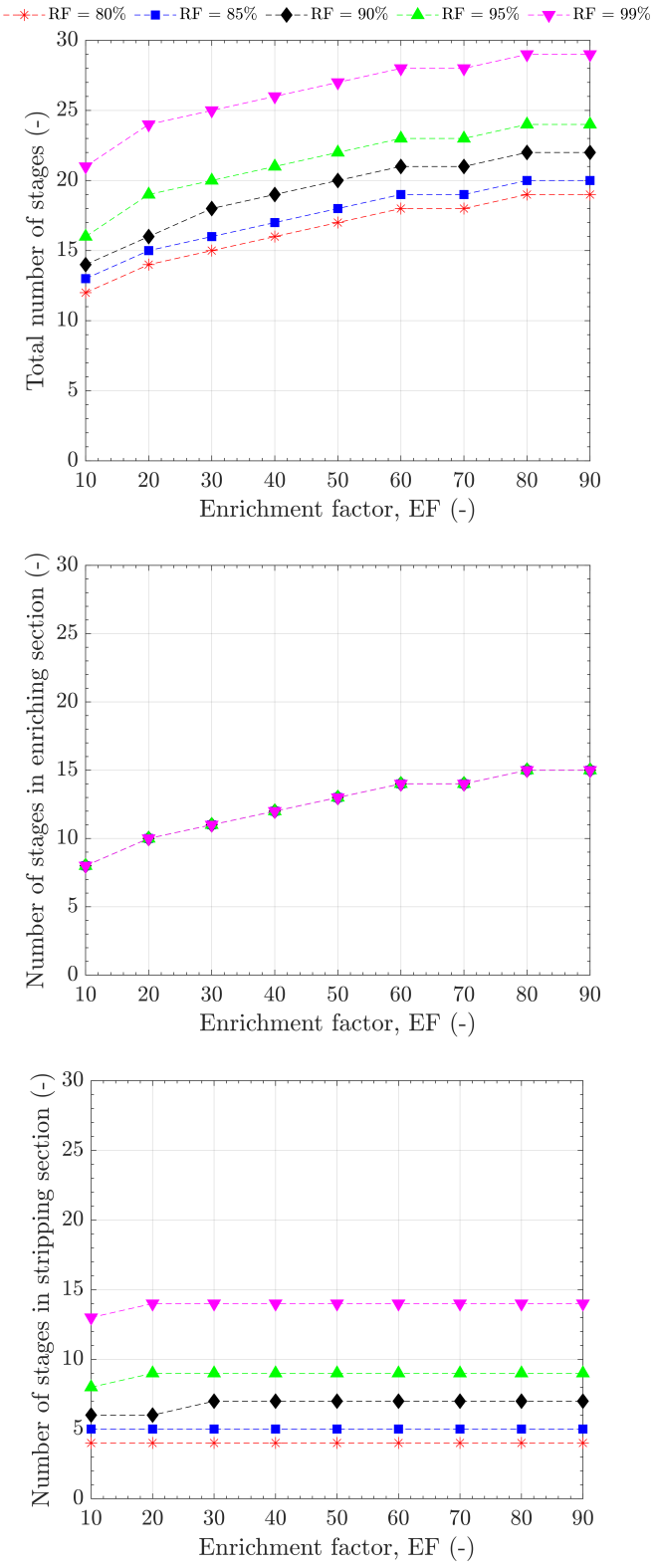

Figure 12: Total number of stages (top), and number of stages in the enriching (middle) and stripping (bottom) sections as a function of EF and RF, obtained for $\gamma = 20$, $\alpha = 2$. $RF = 80\%$: dashed red line with stars; $RF = 85\%$: dashed blue line with squares; $RF = 90\%$: dashed black line with diamonds; $RF = 95\%$: dashed green line with upward triangles; $RF = 99\%$: dashed pink line with downward triangles.

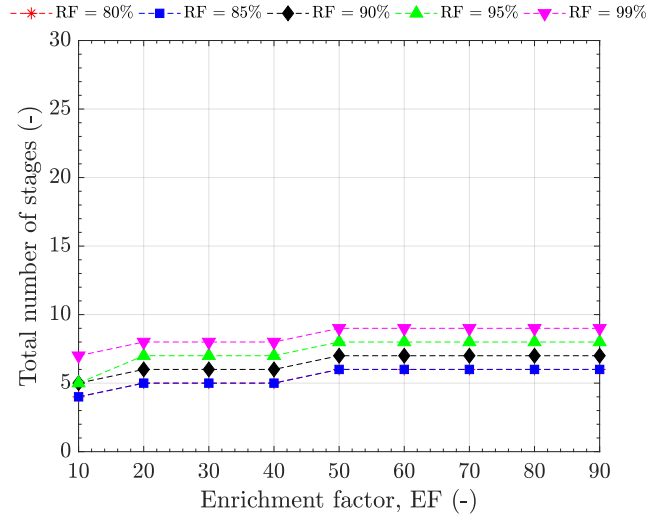

Figure 13: Total number of stages as a function of EF and RF, obtained for $\gamma = 20$, $\alpha = 10$. $RF = 80\%$: dashed red line with stars; $RF = 85\%$: dashed blue line with squares; $RF = 90\%$: dashed black line with diamonds; $RF = 95\%$: dashed green line with upward triangles; $RF = 95\%$: dashed pink line with downward triangles.

4.3.2. *Permeate flow at the last stage*

The permeate flow at the last stage of the cascade ($F_{\mathrm{p,N}}$) is presented as a function of EF and RF for $\gamma = 20$, $\alpha = 2$ and $F_{\mathrm{f,inj}} = 10^4\,\mathrm{m^3/h}$ in figure 14. The dependency of $F_{\mathrm{p,N}}$ with both EF and RF is consistent with the variation of the number of stages in the enriching section: EF significantly impacts $F_{\mathrm{p,N}}$, whereas RF only has a limited influence. Increasing EF for a fixed RF leads to an increase of the number of stages in the enriching section, and thus the permeate flow of stage N decreases: for $RF = 90\%$, $F_{\mathrm{p,N}}$ decreases from $700\,\mathrm{m^3\,h^{-1}}$ to $100\,\mathrm{m^3\,h^{-1}}$ for $EF = 10$ and $EF = 90$, respectively. These results are consistent with the number of stages presented in figure 12.

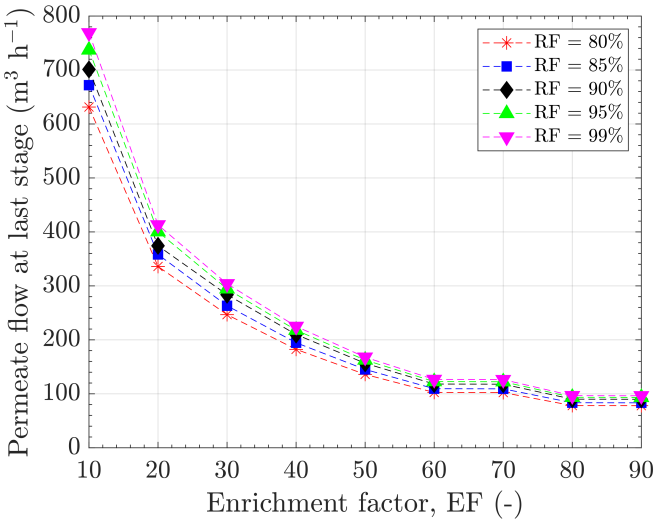

Figure 14: Permeate flow at last stage as a function of EF and RF, obtained for $\gamma = 20$, $\alpha = 2$, $F_{\mathrm{f,inj}} = 10^4\,\mathrm{m^3/h}$. $RF = 80\%$: dashed red line with stars; $RF = 85\%$: dashed blue line with squares; $RF = 90\%$: dashed black line with diamonds; $RF = 95\%$: dashed green line with upward triangles; $RF = 95\%$: dashed pink line with downward triangles.

Increasing the EF requirement brings the benefit of decreasing the permeate flow at thel last stage (i.e., interface with the next system). This may be desired as for instance in the case for a tritium extraction system based on a membrane cascade followed by a palladium-based membrane reactor. On the other side, the lower flow is obtained at the expense of a higher number of stages, which leads to other constraints, such as the space occupied by the system or the power required to run it.

4.3.3. *Power consumption*

In figure 15, the power consumption as a function of EF and for different RF values relative to the reference case ($EF = 20$, $RF = 90\%$) is presented. This plot was obtained for $\alpha = 2$ and $\gamma = 20$. Increasing EF or RF leads to an increase of the power consumption to operate the cascade. These results correlate well with the results presented on figure 12. The stronger dependency of the power consumption with RF is explained by the increasing of the number of stages which results in larger flows along the cascade. Moreover, it should be noticed that this plot gives the relative evolution of the power consumption with EF and RF that applies to any given injection flow.

For higher selectivities, the number of stages is less sensitive to EF and RF and therefore for a high-performing system the increase in power consumption is mitigated.

5. Discussion on the feasibility of a membrane cascade

The results presented in the previous section show the impact of the different design (i.e., EF, RF), operating (i.e., γ) and

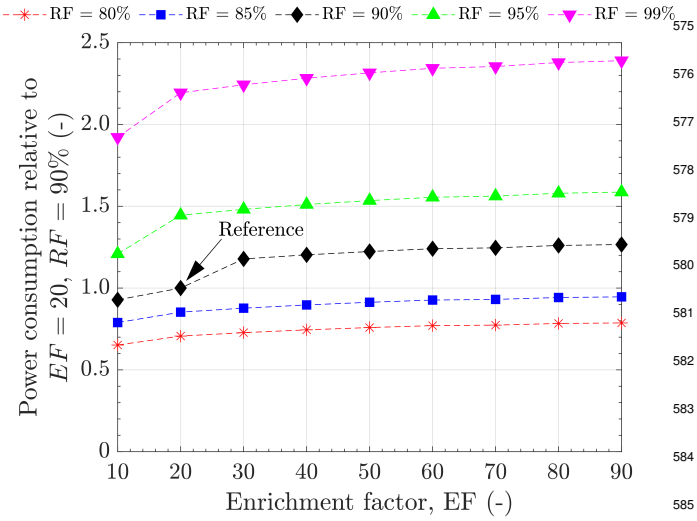

Figure 15: Power consumption relative to the reference case with $EF = 20$ and $RF = 90\%$ as a function of EF and RF. Obtained for $\alpha = 2$ and $\gamma = 20$.

separation (i.e., α) parameters on the number of stages, processing flows, surface area and power consumption of a membrane cascade. These are key information to discuss the feasibility and the interest related to membrane technologies, as fusion requires systems which are as simple as possible, compact, reliable and demonstrate a reasonable energy consumption.

As mentioned above, a multi-stage cascade is required when the separation of a single-membrane is not enough to meet the performance requirements. In the fuel cycle of a fusion reactor, the molecules required for separation (e.g., He, H_2, Ar, N_2, Xe) are rather small in contrast to the pore sizes of the porous (ceramic) membranes available. Therefore, the selectivity should not exceed the so-called Knudsen selectivity, which is determined by the ratio of the molecular masses of the two gas species: $\sqrt{\frac{M_{He}}{M_{H2}}} = 1.41$, $\sqrt{\frac{M_{Ar}}{M_{DT}}} = 2.82$, $\sqrt{\frac{M_{Xe}}{M_{DT}}} = 5.11$ [24, 25]. From figure 5, this would mean that for H_2/He more than 27 stages would be required, whereas for DT/Xe 8 stages would suffice (for $EF = 20$, $RF = 90\%$). However, improvement of the selectivity is possible by exploring other transport mechanisms by surface modification of the membrane. A typical example is the synthesis of molecular-sized surfaces such as zeolites [26]. A modest improvement of the selectivity to 2 was obtained experimentally for H_2/He with MFI zeolite membranes at 298 K (used as reference in this work), due to its adsorption properties, decreasing the number of required stages down to 16 [23]. Higher selectivity values could be obtained for SOD-type zeolite membranes with a pore diameter of 0.27 nm, which is in between the kinetic diameters of He (0.26 nm) and H_2 (0.289 nm) [27, 28]. At these conditions, molecular-sieving mechanism (i.e., separation by size) would occur, decreasing further the number of stages. An example of molecular-sieving with small, non-condensable (permanent) molecules has been reported for H_2/N_2 with carbon membranes ($0.3 - 0.5$ nm), with a very high selectivity of 725 at 298 K [29]. Since the kinetic diameter of Ar (3.54 nm) is similar to that of N_2 (3.72 nm), similar selectivities would be expected for DT/Ar [27]. With these selectivities, only 4 stages would be required for $EF = 20$ and $RF = 90\%$. In fact, this number of stages would already be reached for $\alpha \geq 17$.

Besides the selectivity, the other two factors which have a direct impact on the number of stages and processing components are EF and RF. In the fuel cycle, high-performance cascades are required for a continuous delivery of the desirable tritiated-enriched stream to the interfacing systems. Although $EF = 20$ and $RF = 90\%$ have been considered as reference case (as proposed in [21]), stricter requirements may be required in the future which would lead to a larger number of stages. A direct implication of the number of stages is the space required to accommodate the stages, connecting pipework and process equipment. More importantly, the volume of gas which is continuously processed by the cascade system impacts the tritium inventory. This aspect is very important since one of the arguments in favor of membranes technology (in contrast to more mature technologies) is its potential to minimize tritium inventory, which is of paramount importance in any technology integrating the fuel cyle as discussed in [30, 31]. Therefore, further studies should be conducted to estimate the actual amount of tritium inside the membrane cascade for various number of stages.

Clearly, another aspects impacting the tritium inventory is the initial feeding flow and tritium concentration. As presented

previously, the gas flow downstream of the HCPB breeding blanket is expected to be $10^4\,m^3\,h^{-1}$, which is equivalent to $121\,mol\,s^{-1}$. In contrast, the flow for the separation of the plasma enhancement gases is expected to be $0.14\,mol\,s^{-1}$ [10]. However, since the flow coming from the blanket is expected to have few ppm of HT and the flow from the plasma exhaust is expected to have 99% of DT, a higher tritium inventory may be expected despite the lower flow for the latter case (provided they have the same number of stages) [32]. Moreover, the feed flow has also a direct impact on the compression power. The values presented in the plot of figure 11 show that, for $\alpha < 3$, the power required is more than 1% of the net power expected for the EU-DEMO (3 GW [5]), which may not be feasible. Nevertheless, a strong power reduction would be attained with higher selectivity membranes (for $\alpha > 10$ the power required would be below 0.2%). Furthermore, the feed flow has a direct impact on the required surface area per stage which will impact the volume of the vessel accommodating the membrane.

Last but not least, the input flows impact directly the permeate and retentate flows downstream of the cascade. Regardless of the selectivity, the same order of magnitude is expected for the downstream flows (for $10^4\,m^3\,h^{-1}$, the highest flow reduction on the permeate side is around 100). Thus, if the interfacing systems require smaller flows for optimum sizing, operation and costs, the feeding flow of the cascade should be reduced. However, this flow reduction is limited by the requirements of the systems upstream (e.g., purging of the breeding blanket for tritium recovery).

In sum, the main limiting factors for a cost-efficient, small, yet high-performing, membrane cascade are the selectivity α, feed flow $F_{f,inj}$ and required performance parameters EF and RF. Moreover, the design of an optimized cascade has to take into account the requirements of the interfacing systems in the fuel cycle of the fusion reactor.

6. Conclusions

This paper presents as numerical code developed to size a multi-stage membrane system depending on the following input parameters: selectivity α, pressures-ratio γ enrichment factor EF and recovery fraction RF. A sensitivity study was performed using this tool to determine the most impacting parameters on the dimensioning of membrane cascade systems in view of the fuel cyle of fusion reactors.

The selectivity α, given by the ratio of the permeances of the two gas species, and the pressure-ratio γ across the membrane have a direct impact on the achievable separation of a single-stage and thus on the number of stages needed to meet certain performance parameters. These parameters are the enrichment factor EF and RF, and the higher these values the more number of stages is required. In the case of the TER for the HCPB blanket, $EF = 20$ and $RF = 90\%$ have been used as reference, which would lead to a minimum number of 16 stages for $\alpha = 2$ and 6 for $\alpha = 10$. For larger selectivities, the number of stages required would be reduced to 4. The injection flow has a direct impact on the membrane surface-area and compression power necessary to run a cascade. For instance, with $\alpha = 10$ (i.e., 6 stages) injection flows of $10^4\,m^3h^{-1}$ may require $10^2\,m^2$ and 4 MW. Furthermore, the higher the injection flows the larger is the footprint of the system and hence the higher is the tritium inventory, which is a key aspect for the overall tritium management in the fuel cycle of the fusion reactor.

Due to the similar sizes of the molecules expected in a fusion reactor, the selectivities are rather limited for the majority of the membranes available. The increase of the selectivities towards the range of interest (i.e., lowest number of stages) can be achieved by either exploring the different adsorption properties of those molecules onto materials or molecular-sieving. These separation mechanisms could be achieved with microporous materials such as zeolite or carbon membranes.

Acknowledgements

This work has been carried out within the framework of the EUROfusion Consortium and has received funding from the Euratom research and training programme 2014-2018 under grant agreement No 633053. The views and opinions expressed herein do not necessarily reflect those of the European

Commission.

Appendix A. Separation factor dependency with α, γ and y_p

A two-component (a and b) gas stream feeding a given membrane permeates through it with a total flow F_p. Assuming a module with perfect mixing, where the concentrations in the lumen ($x_{r,a}$ and $x_{r,b}$) and permeate ($y_{p,a}$ and $y_{p,b}$) sides are constant, equations (A.1) and (A.2) apply for the component flows permeating the membrane.

$$y_{p,a}F_p = \frac{\Pi_a p_f}{t}(x_{r,a} - \gamma^{-1}y_{p,a})A \quad (A.1)$$

$$y_{p,b}F_p = \frac{\Pi_b p_f}{t}(x_{r,b} - \gamma^{-1}y_{p,b})A \quad (A.2)$$

Since $y_{p,a} = 1 - y_{p,b} \equiv y_p$ and $x_{r,a} = 1 - x_{r,b} \equiv x_r$, using equation (9), and dividing equation (A.1) by (A.2), the relation (A.3) is obtained. Then, x_r, written as function of S_{stg} and y_p with equation (3), must be replaced in (A.3). After some algebra, equation (A.4) is finally obtained which expresses S_{stg} as a function of α, γ and y_p.

$$\frac{y_p}{1-y_p} = \alpha\frac{x_r - \gamma^{-1}y_p}{(1-x_r) - \gamma^{-1}(1-y_p)} \quad (A.3)$$

$$S_{stg} = \frac{\alpha - y_p(\alpha-1)\gamma^{-1}}{1 + (1-y_p)(\alpha-1)\gamma^{-1}} \quad (A.4)$$

Appendix B. Determination of cut using species concentrations

From the global mass-balance ($F_f = F_p + F_r$) and the component mass-balance ($F_f x_f = F_p y_p + F_r x_r$), equations, relation (B.1) follows.

$$\frac{F_p}{F_r} = \frac{x_f - x_r}{y_p - x_f} \quad (B.1)$$

Since $\nu = \frac{F_p}{F_p+F_r}$, then $\frac{F_p}{F_r} = \frac{\nu}{1-\nu}$. Thus, by equating the latter with (B.1), equation (19) is obtained after some algebra.

References

[1] I. Cristescu, et al., Commissioning of water detritiation and cryogenic distillation systems at TLK in view of ITER design, Fusion Engineering and Design 82 (2007) 2126–2132.

[2] M. Glugla, et al., The ITER tritium systems, Fusion Engineering and Design 82 (5-14) (2007) 472–487.

[3] A. Ciampichetti, et al., Conceptual design of tritium extraction system for the european HCPB test blanket module, Fusion Engineering and Design 87 (6-6) (2012) 620–624.

[4] D. Demange, et al., A new combination of membranes and membrane reactors for improved tritium management in breeder blanket of fusion machines, Fusion Engineering and Design 86 (9-11) (2011) 2312–2316.

[5] G. Federici, et al., European DEMO design strategy and consequences for materials, Nuclear Fusion 57 (2017) 092002.

[6] A. Brunetti, et al., Membrane technologies for CO2 separation, Journal of Membrane Science 359 (2010) 115–125.

[7] V. Violante, et al., Membrane separation technologies: their application to the fusion reactor fuel cycle, Fusion Engineering and Design 22 (3) (1993) 257–263.

[8] A. Basile, et al., Membrane integrated system in the fusion reactor fuel cycle, Catalysis Today 25 (3-4) (1995) 321–326.

[9] S. Tosti, A. Pozio, Membrane processes for the nuclear fusion fuel cycle, Membranes 8 (4) (2018) 1–14.

[10] S. Tosti, et al., Ceramic membranes for processing plasma enhancement-gases, Fusion Engineering and Design 124 (2017) 928–933.

[11] D. Demange, et al., Zeolite membranes and palladium membrane reactor for tritium extraction from the breeder blankets of ITER and DEMO, Fusion Engineering and Design 88 (2013) 2396–2399.

[12] A. F. Ismail, et al., Gas Separation Membranes: polymeric and inorganic, Springer, 2015.

[13] K. K. Sirkar, Separation of Molecules, Macromolecules and Particles: Principles, Phenomena and Processes, Cambridge University Press, 2014, Ch. 9. Cascades, pp. 812–818.

[14] R. W. Baker, Membrane Technology and Applications, John Wiley & Sons Ltd, 2012, Ch. 8. Gas Separation, pp. 325–378.

[15] S. Weller, W. A. Steiner, Separation of gases by fractional permeation through membranes, Journal of Applied Physics 21 (1950) 279–283.

[16] T. C. Merkel, et al., Power plant post-combustion carbon dioxide capture: An opportunity for membranes, Journal of Membrane Science 359 (2010) 126–139.

[17] M. Ohno, et al., Gas separation performance of tapered cascade with membrane, Journal of Nuclear Science and Technology 15 (6) (1978) 411–420.

[18] M. Binns, et al., Strategies for the simulation of multi-component hollow fibre multi-stage membrane gas separation systems, Journal of Membrane Science 497 (2016) 458–471.

[19] G. Towler, R. Sinnott, Chemical Engineering Design: Principles, Practice

and Econmics of Plant and Process Design, 2nd edition, Elsevier, Ltd., 2013, pp 1221 - 1222.

[20] H. Nguyen-Schaefer, Rotordynamics of Automotive Turbochargers, Springer-Verlag, 2012, Ch. Thermodynamics of Turbochargers, pp. 21–24.

[21] O. Borisevich, et al., Zeolite membrane cascade for tritium extraction and recovery systems, Fusion Science and Technology 67 (2) (2015) 262–265.

[22] F. Hernández, et al., A new HCPB breeding blanket for the EU DEMO: Evolution, rationale and preliminary performances, Fusion Engineering and Design 124 (2017) 882–886.

[23] O. Borisevich, et al., Experimental study of permeation and selectivity of zeolite membranes for tritium processes, Fusion Engineering and Design 98-99 (2015) 1755–1758.

[24] K. Li, Ceramic Membranes for Separation and Reaction, John Wiley & Sons, 2007, Ch. 4. Transport and Separation of Gases in Porous Ceramic Membranes, pp. 97 – 134.

[25] National Institute of Standards and Technology, NIST Chemistry WebBook, online, visite on 04/11/2018, URL: `https://webbook.nist.gov/chemistry/mw-ser/`.

[26] N. Kosinov, et al., Recent developments in zeolite membranes for gas separation, Journal of Membrane Science 499 (2016) 65–79.

[27] S. M. Auerbach, et al. (Eds.), Handbook of Zeolite Science and Technology, Marcel Dekker, Inc., 2003.

[28] S. Khajavi, et al., Preparation and performance of H-SOD membranes: a new synthesis procedure and absolute water preparation, in: R. Xu, et al. (Eds.), From Zeolites to Porous MOF Materials - the 40th Anniversary of International Zeolite Conference, 2007.

[29] M. A. L. Tanco, et al., Composite-alumina-carbon molecular sieve membranes prepared from novolac resin and boehmite. Part II: Effect of the carbonization temperature on the gas permeation properties, International Journal of Hydrogen Energy 40 (2015) 3485–3496.

[30] B. Bornschein, et al., Tritium management and safety issues in ITER and DEMO breeding blankets, Fusion Engineering and Design 88 (2013) 466–471.

[31] Y. Hörstensmeyer, et al., Analysis of the EU-DEMO fuel cycle elements: Intrinsic impact of technology choices, Fusion Engineering and Design in press.

[32] F. Franza, et al., Tritium transport analysis in HCPB DEMO blanket with the FUS-TPC code, Fusion Engineering and Design 88 (9-10) (2013) 2444–2447.